Structure and Mechanism of the Farnesyl Diphosphate Synthase from *Trypanosoma cruzi:* Implications for Drug Design

Sandra B. Gabelli,[1] Jason S. McLellan,[1] Andrea Montalvetti,[3,5] Eric Oldfield,[2] Roberto Docampo[3,4] and L. Mario Amzel[1]*

[1]*Department of Biophysics and Biophysical Chemistry, Johns Hopkins School of Medicine, Baltimore, Maryland 21205*
[2]*Department of Chemistry, University of Illinois at Urbana–Champaign, Urbana, Illinois 61801*
[3]*Department of Pathobiology and Center for Zoonoses Research, University of Illinois at Urbana–Champaign, Urbana, Illinois 61802*
[4]*Center for Tropical and Global Emerging Diseases and Department of Cellular Biology, University of Georgia, Athens, Georgia 30606*
[5]*Funcacion Instituto Leloir, Avda Patricias Argentinas 435. C1405BWE, Buenos Aires, Argentina.*

ABSTRACT ***Typanosoma cruzi*, the causative agent of Chagas disease, has recently been shown to be sensitive to the action of the bisphosphonates currently used in bone resorption therapy. These compounds target the mevalonate pathway by inhibiting farnesyl diphosphate synthase (farnesyl pyrophosphate synthase, FPPS), the enzyme that condenses the diphosphates of C_5 alcohols (isopentenyl and dimethylallyl) to form C_{10} and C_{15} diphosphates (geranyl and farnesyl). The structures of the *T. cruzi* FPPS (*Tc*FPPS) alone and in two complexes with substrates and inhibitors reveal that following binding of the two substrates and three Mg^{2+} ions, the enzyme undergoes a conformational change consisting of a hinge-like closure of the binding site. In this conformation, it would be possible for the enzyme to bind a bisphosphonate inhibitor that spans the sites usually occupied by dimethylallyl diphosphate (DMAPP) and the homoallyl moiety of isopentenyl diphosphate. This observation may lead to the design of new, more potent anti-trypanosomal bisphosphonates, because existing FPPS inhibitors occupy only the DMAPP site. In addition, the structures provide an important mechanistic insight: after its formation, geranyl diphosphate can swing without leaving the enzyme, from the product site to the substrate site to participate in the synthesis of farnesyl diphosphate. Proteins 2006;62:80–88.**

Key words: farnesyl diphosphate synthase; geranyl diphosphate; mevalonate pathway; bisphosphonate; risedronate; alendronate; conformational change; *Trypanosoma cruzi*; Chagas disease

INTRODUCTION

American trypanosomiasis (Chagas disease) is an endemic parasitic disease that affects an estimated 16–18 million individuals across Latin America.[1] Of these, 15–20% can be expected to have clinical manifestations at any given time. Because of the possibility of transmission through blood transfusion, it is also becoming a health concern in the United States. Chagas disease is caused by *Trypanosoma cruzi,* a flagellated protozoan that is transmitted to humans in the feces of its triatomine insect vector. The life cycle of *T. cruzi* includes obligatory stages in the host and in the insect. In the host it has two forms: an intracellular replicative form (amastigote), and a nonreplicative bloodstream form (trypomastigote) that can invade host cells. Two forms also occur in the vector: one replicative (epiastigote), and one nonreplicative (metacyclic trypomastigote). These forms differ in size, subcellular organization, antigenicity, and metabolism.

In humans, Chagas disease goes through three phases: an acute phase, a long asymptomatic phase, and a chronic phase that, if it develops, can lead to sudden death. Two drugs, benznidazole and nifurtimox are currently used for the treatment of the disease.[2] They are effective for patients in the acute phase but are of little or no use in the treatment of chronic patients.[3] The need for new, more effective, less toxic drugs against *T. cruzi* cannot be overstated.

Recently bisphosphonates have been shown to be active against *T. cruzi*, both in vitro and in vivo, suggesting their potential as a new family of anti-Chagasic compounds.[4,5] In bisphosphonates, the bridging oxygen atom of the diphosphate moiety is replaced by a carbon atom carrying various substituents. Compounds in this family are potent inhibitors of bone resorption and are in clinical use for the treatment and prevention of osteoporosis, hypercalcemia, Paget's disease, tumor metastasis in bone, and other related diseases.[6,7] During many years of use, bisphosphonates have demonstrated low toxicity.

Grant sponsor: NIH; Grant numbers: GM066895 (L.M.A.), GM65307 (E.O.) (from the National Institute of General Medical Sciences).

*Correspondence to: L. Mario Amzel, Department of Biophysics and Biophysical Chemistry, Johns Hopkins School of Medicine, 725 North Wolfe Street, Baltimore, MD 21205.
E-mail: mario@neruda.med.jhmi.edu

Received 9 May 2005; Revised 1 July 2005; Accepted 27 July 2005

Published online 15 November 2005 in Wiley InterScience (www.interscience.wiley.com). DOI: 10.1002/prot.20754

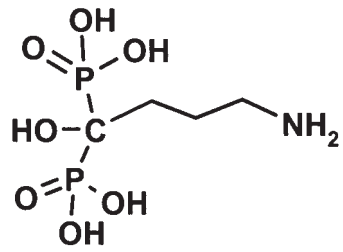

alendronate

Scheme 2

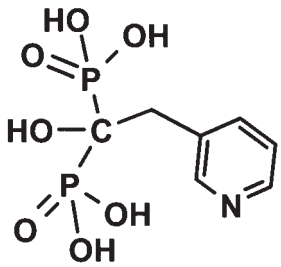

risedronate

Scheme 3

Bisphosphonates have been shown to target the mevalonate pathway.[8] In particular, they inhibit farnesyl diphosphate synthase (FPPS), the enzyme that catalyzes the condensation of isopentenyl diphosphate (IPP) and dimethylallyl diphosphate (DMAPP) to form geranyl diphosphate (GPP) and subsequently farnesyl diphosphate (FPP).[9] FPP and GPP are precursors for the biosynthesis of most of the isoprenoid compound family. Importantly, FPP is the branching point in the mevalonate pathway leading to farnesylated proteins and to the biosynthesis of dolichols and sterols, such as cholesterol and ergosterol.

Pamidronate (Aredia™) and alendronate (Fosamax™), two nitrogen-containing bisphosphonates, are active in mice against the intracellular form of *T. cruzi* (amastigote) with IC_{50} values of 60 and 147 μM and low toxicity.[4,10,11] Furthermore, development of the disease in mice in the acute stage of a *T. cruzi* infection can be effectively arrested using intravenous injection of pamidronate. *Tc*FPPS, the farnesyl diphosphate synthase of *T. cruzi*, has been shown to be the most likely target of the nitrogen-containing bisphosphonates.[4,5,9,12] In this article we describe the three-dimensional structure of *Tc*FPPS, alone and in two complexes—one with risedronate (Scheme 3), DMAPP, and Mg^{2+}, the other with alendronate (Scheme 2), IPP, and Mg^{2+}—determined by single-crystal X-ray diffraction. These structures represent an important step in the development of new, more effective anti-Chagasic bisphosphonates.

RESULTS AND DISCUSSION

Overall structure of the *T. cruzi* FPPS

The structure of the *Tc*FPPS, determined to 2.0-Å resolution (R = 17%, R_{free} = 22%), can be best described as a two-helix N-terminal hairpin followed by a central eight-helix bundle, analogous to those of the equivalent enzymes from chicken and *Escherichia coli*.[13,14] The conserved DDXXD motifs (residues 98–102 and residues 250–254) are contained in helices D and H of the central core (Fig. 1). The eight helices in the bundle are connected by loops, with two exceptions. Connecting helices H and I are three short helices: two form an antiparallel hairpin that protrudes from the core, perpendicular to the eight-helix bundle, the other completes the connection to the bundle. Between helices F and G the enzyme contains an 11-residue insertion (residues 179–189) that is unique to trypanosomatid FPPSs. This insertion folds as a tight loop, with a reverse turn at Pro182. This sequence is also present in *T. brucei* FPPS, although its conformation in the structure appears different, due perhaps to the lack of experimental phases in the 3.6 Å *T. brucei* structure.[15]

In the crystals, the two monomers in the *Tc*FPPS dimer are related by a crystallographic twofold axis. Formation of the dimer buries 6028 $Å^2$. The trypanosome-specific insertion reaches from one monomer to the other and contributes to the area of contact between monomers in the dimer (Fig. 2).

Structure of the Complex of *Tc*FPPS with Alendronate, IPP, and Mg^{2+}

The structure was determined at 2.5-Å resolution and refined to an R-value of 21% (R_{free} = 28%) with excellent geometry (Table I). The crystal form, obtained by crystallization of the complex, is different from but related to that of the apo enzyme. The most important difference is a reduction of 12 Å in the cell dimension of the c-axis. This change reflects a general conformational change that occurs in the protein upon complex formation: the protein undergoes a hinge-like motion of 6.5° (maximum displacement ~4 Å) that closes the structure around the ligands. This change is reflected most noticeably in the position of the loops connecting helices D and E and helices G and H. These movements position Arg 107 and Lys 264 between the diphosphates of the two substrates. In addition, the C-terminal motif RXK (residues 360–362; conserved in all FPPS except the bacterial enzymes), that is disordered in the apo enzyme, becomes well order as a result of newly formed H-bond interactions with the IPP diphosphate through residues Arg 360 and Lys 362 (Fig. 3). This interaction provides a rationale for the observation that the mutation to Ala of the arginine residue of *B. stearothermophilus* equivalent to Arg 360 increases the IPP K_m of the FPPS by threefold and does not change the GPP K_m.[16] This observation was puzzling when only the apo structure was available. Further comparison with the apo structure shows that the side chains of Asp 98 and Asp 250 rotate by 90° about χ_1 to accommodate metal binding. In making this rotamer change, Asp 250 breaks a salt bridge it makes with Arg 360 in the apo structure.

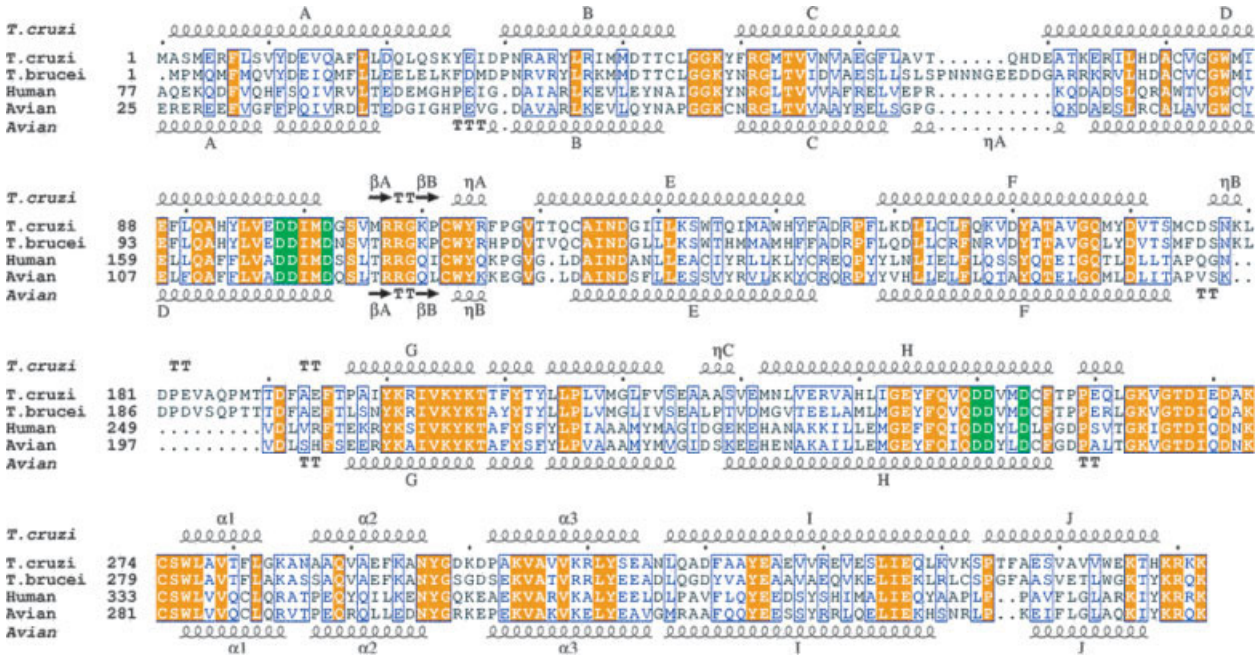

Fig. 1. Alignment of farnesyl pyrophosphate synthase sequences. The secondary structure elements of the *T. cruzi* enzyme and of the avian enzyme are shown at the top and the bottom, respectively. Fully conserved amino acids are shown in orange and conservative substitutions in blue. The 11-residue insertion between helices F and G, typical of trypanosomatids, is evident in this alignment. The insertion folds as tight loop that interacts with the other monomer of the dimer. Because helices α1, α2, and α3 are not present in the bacterial enzymes, they were named this way to maintain equivalence of helices I and J between eukaryotic and bacterial enzymes.

The catalytic site of *Tc*FPPS has two distinct regions, one (homoallylic) occupied by IPP, the other (allylic) by the alendronate and three Mg^{2+} ions. The diphosphate of IPP binds pointing away from the alendronate and is contacted by charged residues: Arg 360, Lys 362, and Arg 51. In addition, the α-phosphate contacts the guanidinium group of Arg 108 and the main chain amide of Lys 48. The isopentenyl group extends towards the alendronate with its terminal methylene pointing toward the inhibitor and located at 3.34 Å from the alendronate OH. Alendronate binds to the same site occupied by thiolo-DMAPP in the structure of the *E. coli* FPPS.[14] The butylammonium portion of the inhibitor extends away from the IPP with the ammonium nitrogen in close proximity to the Oγ of Thr 208, the carbonyl oxygen of Lys 207, the OH of Tyr 211 and the Oε of Gln 167. The OH of the alendronate makes an H-bond to Asp 250. Loss of this interaction is likely responsible for the slightly lower affinity shown by bisphosphonates that lack the OH group at C1.[12] The two phosphonate groups interact mainly with the three Mg^{2+} ions, which in turn, interact with the protein through three aspartates—two from the first conserved DDXXD motif (Asp 98 and 102), and one from the second (Asp 250). Two oxygens, one from each phosphonate, bind one of the Mg^{2+} ions (Mg—O distances of 1.83 and 2.03 Å). Another Mg^{2+} ion also binds two oxygens (Mg—O distances of 1.92 and 2.02 Å). The third oxygen of one phosphonate forms H-bonds to two positively charged residues Arg 107 and Lys 264. The third oxygen of the other phosphonate makes an H-bond with Lys 207.

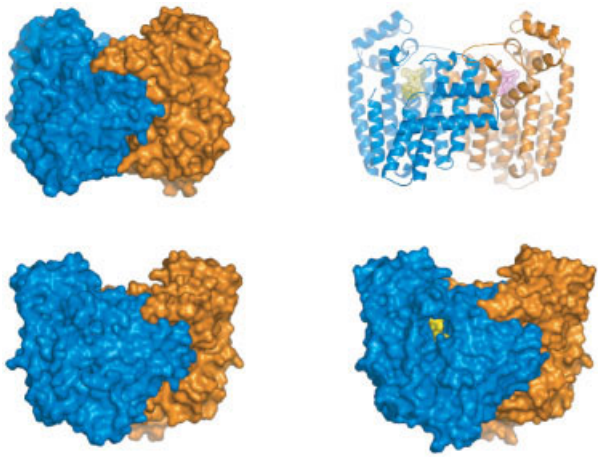

Fig. 2. Surface and ribbon representation of the *T. cruzi* FPPS dimer. (**a**) Surface view shows the 11-residue loop of one monomer interacting with the second monomer. (**b**) Ribbon representation shown in the same orientation as (**a**). A mesh representation of the envelope of the active site is shown in both monomers (yellow and pink). (**c**) Surface representation of the FPPS dimer in the closed conformation (complex structure). (**d**) Surface representation of the FPPS dimmer in the open conformation (apo structure). Drawings (**c**) and (**d**) are in same orientation. The substrate binding site shown in yellow is seen only in the open conformation because only in this conformation it is accessible to the solvent.

Structure of the Complex of *Tc*FPPS with Risedronate, DMAPP, and Mg^{2+}

The structure of this complex was determined to 1.9-Å resolution and refined to an *R*-value of 17% (R_{free} = 23%) with excellent geometry (Table I). The crystals of this

TABLE I.

Crystal	Selenomethionyl			Native	Risedronate Dmapp Mg	Alendronate IPP Mg
Space group				$P6_122$		
Unit cell	$a,b = 57.9$ Å, $c = 396.9$ Å			$a,b = 57.9$ Å, $c = 397.6$ Å	$a,b = 58.1$ Å, $c = 389.5$ Å	$a,b = 103.2$ Å $c = 385.2$ Å
Data collection statistics						
X-ray source	BNL-X25			BNL-X4a	BNL-X25	BNL-X25
Wavelength (Å)	0.9791(pk)	0.9793(edge)	0.96(remote)	0.9792	1.1	1.1
Resolution (Å)	50.0 – 2.4	50.0 – 2.4	50.0 – 2.4	65.0 – 2.01	50.0 – 1.95	50.0 – 2.5
HighRes shell (Å)	2.51–2.4	2.51–2.4	2.51–2.4	2.10–2.01	2.02–1.95	2.59–2.5
Measured reflections	244,951	242,905	264,428	200,492	264,824	622,749
Unique reflections	16,394	16,414	17,475	23,087	29,502	43,448
Completeness (%)	99.7 (99.9)	99.6 (99.9)	99.6(98.9)	93.9 (91.0)	97.96 (89.1)	99.8 (100.0)
R_{merge} (%)	12.0 (33.0)	11.4 (38.0)	9.6 (32.6)	9.9 (36.0)	9.6 (51.0)	13.0 (55.0)
Average I/σ	14.9	13.2	15.1	20.4	12.4	10.7
Redundancy	14.9 (13.1)	14.8 (12.9)	15.1 (12.6)	8.6 (8.0)	8.9	12.9
Mosaicity (°)	0.30	0.29	0.31	0.45	0.30	0.50
Refinement						
R_{cryst}	0.21			0.17 (0.21)	0.17 (0.22)	0.21 (0.29)
R_{free}	0.28			0.22 (0.29)	0.23 (0.32)	0.28 (0.34)
RMS deviations						
Bonds (Å)	0.008			0.031	0.028	0.019
Angles (°)	1.2			2.0	2.2	2.0
Monomer in Asu	1			1	1	3
Total atoms	2987			3163	3336	8894
Water molecules	107			288	402	119
Ligands (per monomer)	1 SO_4			2 SO_4	1 SO_4	1 SO_4
	—			—	1 Ris,1 DMAPP	1 Ale, 1 IPF
Metals (per monomer)	—			—	3 Mg^{+2}	3 Mg^{+2}
B average	35.50 $Å^2$			31.35 $Å^2$	26.05 $Å^2$	41.00 $Å^2$

complex, obtained by soaking crystals of the apo enzyme in mother liquor containing the ligands, also show an 8 Å shortening of the crystallographic c axis. This shortening is a consequence of the same overall closing of the structure observed in the other complex.

Because the structure of this complex was determined at high resolution (Fig. 3), it presented the opportunity to analyze the details of the interactions of the inhibitor with the protein. After refining the structure with strong planarity constraints, the $2F_o - F_c$ maps contoured at high density values show bulging of the density away from the pyridyl ring plane at the position of the ring nitrogen, suggesting a partial sp^3 character of this nitrogen. Several interactions may be responsible for this effect. An oxygen atom of one of the phosphonate phosphates that points back towards the ring, is at only 2.9 Å from the carbon at the ortho position of the pyridyl moiety. The nitrogen is at H-bonding distance of Thr 208 (2.87 Å) and at a short distance of Tyr 211 (3.47 Å).

Alignment of this structure with that of the alendronate-containing complex shows that the equivalent risedronate atoms fully overlap with those of alendronate and make all the same contacts, including those with the three metal ions. Surprisingly, DMAPP, which would normally bind to the site occupied by alendronate, binds in this complex in the IPP site (homoallylic) (Fig. 3). It does not, however, overlap *all* the atoms of IPP. This mode of binding takes place with low affinity,[17,18] and was probably allowed by the high concentration of DMAPP present in the crystal (4 mM). The β-phosphates of DMAPP and IPP bind to the same position, but the α-phosphates and the rest of the chains diverge from each other: the bridging oxygen of DMAPP is at 180° from the one of IPP, and the pyrophosphate folds back at the α-phosphate so that the dimethyl groups overlap the position of the ester bond of IPP.

This structure provides a plausible answer to a question about the specificity of FPPS that has eluded explanation. The two substrates of the enzyme IPP and DMAPP are structural isomers: they contain the same atoms with the same connectivity. The only difference is the position of the double bond. It is not likely that the enzyme can distinguish the small differences in positions of the atoms that result from the differences in bond lengths. However, it is clear from the structure of this complex that although DMAPP can bind in the IPP site, it cannot bind in the same position as IPP: IPP binds with the C1—C2 and the C3—C4 (or C5) bonds in a configuration 16° from planarity around the C2—C3. This departure from planarity is necessary because of a close interaction with Phe 246 (3.2 Å), Tyr 211 (3.2 Å), Leu 95 (4.0 Å), and a 3.5-Å contact between the Nϵ of Lys 264 and the C1 of IPP. The C2—C3 bond of DMAPP is, however, a double bond, so all five carbon atoms lie in the same plane.

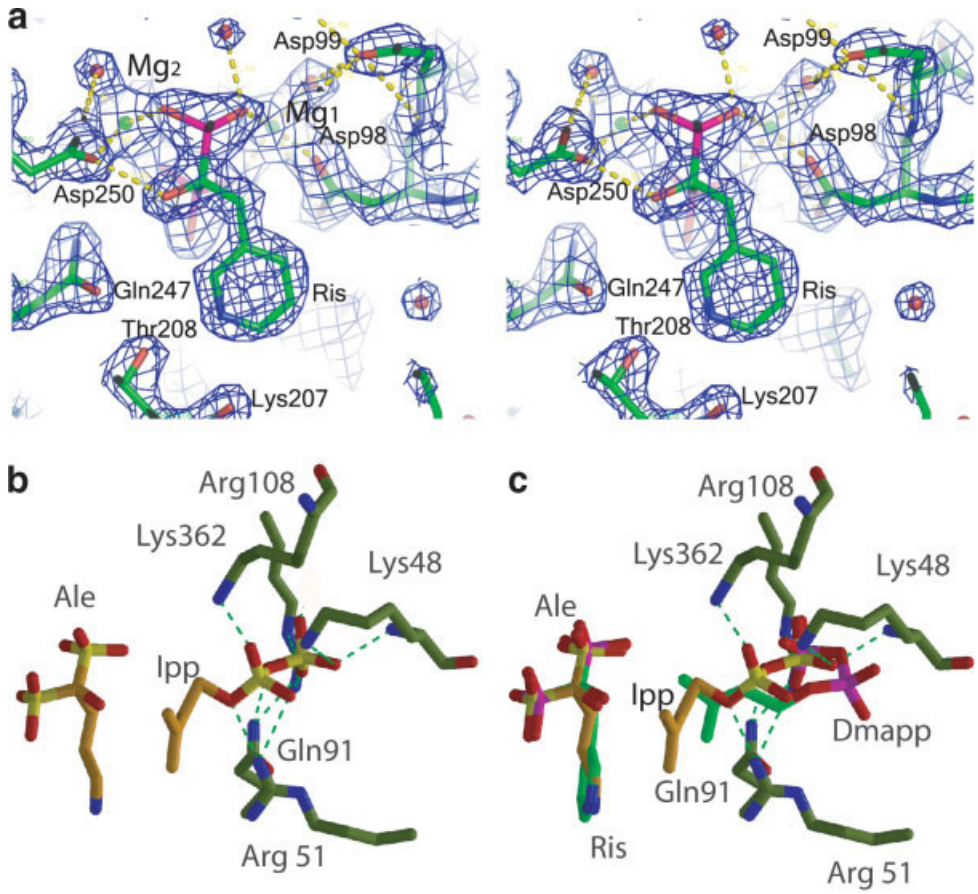

Fig. 3. Structures of the complexes of *T. cruzi* FPPS with inhibitor, substrate, and Mg^{2+}. (**a**) The electron density and the model of the risedronate with its surrounding residues is shown in stereo in the complex of *T. cruzi* FPPS with risedronate, DMAPP, and magnesium. Carbon atoms are shown in green, nitrogens in blue, and oxygens in red. Magnesium ions are shown as small green spheres and water molecules as red spheres. Some of the important H-bonds are indicated by dotted yellow lines. (**b**) Residues at hydrogen bonding distance of IPP in the complex structure of the *T. cruzi* FPPS with alendronate, IPP, and magnesium. All the residues in contact with Alendronate, Arg 360, magnesium atoms, and water molecules have been omitted for clarity. (**c**) Overlap of both complex structures of *T. cruzi* FPPS. For the alendronate–IPP–Mg structure carbons are shown in orange and phosphates in yellow. For the risedronate–DMAPP–Mg structure carbons are shown in bright green and phosphates in magenta. Only side chains of the complex structure of the *T. cruzi* with FPPS with alendronate, IPP, and magnesium are shown as in (**b**).

Thus, discrimination between the substrates involves binding IPP in a configuration that cannot be adopted by the other substrate, DMAPP.

Coordination of the Mg^{2+} Ions

The coordination of the Mg^{2+} ions in both complexes is highly similar. All three Mg^{2+} ions are octahedrally coordinated by phosphonate oxygens, aspartyl carboxylates, and water molecules (Fig. 4). The ligands of Mg 1 are one oxygen of each phosphonate in risedronate (or alendronate), the carboxylates of Asp 102 and Asp 98 (both of the first DDXXD motif), and two water molecules. Mg 2 also has two phosphonate–oxygen ligands, but the other four positions are occupied by the carboxylate of Asp 250 (of the second DDXXD motif) and three water molecules. Mg 3 is coordinated by the same two aspartates of the first DDXXD motif (Asp 98 and Asp 102), one phosphonate oxygen, and three water molecules. All Mg—O distances fall within the range 1.95 to 2.24 Å.

Notably, all three Mg^{2+} ions bind to the diphosphate of the allylic site (alendronate and risedronate in the structures described here), and no metal ion is associated with the IPP (homoallylic site). This structural feature is a consequence of a mechanistic requirement. Because the diphosphate of the allylic substrate is the leaving group of the reaction, coordination to the ions will favor release of this group. Furthermore, if as proposed, the reaction takes place with a dissociative mechanism, these ions will favor ionization of the allylic substrate. The fact that many of the ligands to the Mg^{2+} ions are provided by DMAPP explains why magnesium binding only takes place in the presence of substrate.[17]

General Properties of the Catalytic Site

Each of the two regions of the catalytic site of FPPS (allylic diphosphate and homoallylic diphosphate sites) can be considered as subdivided into two subsites. The two subsites of the allyl diphosphate binding region are: the

PPAl subsite, which binds the diphosphate moiety of the acceptor molecule (either DMAPP or GPP), and the Al subsite, which binds the hydrocarbon chain [Fig. 5(a, b)].

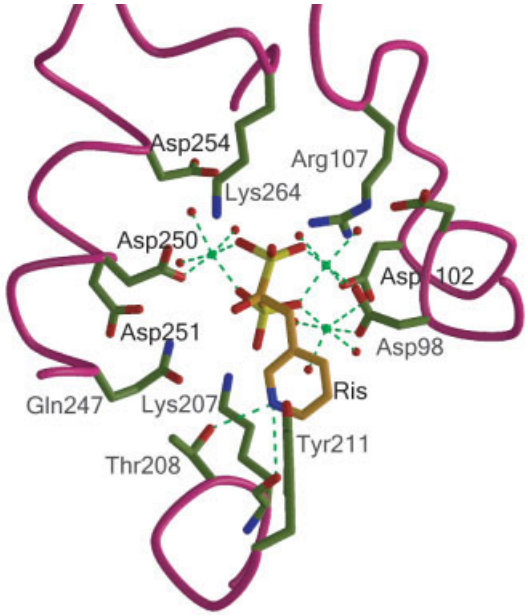

Fig. 4. Coordination of the three Mg^{2+} ions and risedronate. Water molecules and magnesium ions are shown as in Figure 3. Hydrogen bonds as well as interactions with the magnesium ions are shown as green dashed lines.

Because subsite PPAl contains the diphosphate that will leave the molecule as part of the reaction, it also contains the three Mg^{2+} ions that participate in catalysis. Subsite Al requires that the five carbon atoms adjacent to the phosphate be coplanar. The homoallyl diphosphate binding region has two distinct subsites: one, subsite PPHAl, binds the diphosphate of the IPP, and the other, subsite HAl, binds the isopentenyl moiety.

Mechanistic Insights

The mechanism proposed for the FPPS reaction (Scheme 1) requires the abstraction of the H_R proton of C-2 of the carbenium product intermediate.

Although the pKa of the intermediate is low, it is still necessary to provide a base for the abstraction of the proton and for providing a path to the bulk solvent. The structures presented here show that one of the oxygens of the phosphonate of alendronate is at 3.7 Å of the H_R proton of IPP. This arrangement indicates that in the last step of the reaction, the diphosphate that separates from the second substrate will be ideally positioned to abstract the proton from the IPP, as was suggested by Cornforth.[19] As this pyrophosphate is released, it will carry the abstracted proton to the bulk solvent. Instances of substrate/product phosphates acting as the catalytic bases in enzyme catalyzed reactions have been postulated before, including for the mechanism of the *E. coli* FPPS.[14]

The structures presented here, together with previously reported data,[20] suggest that the two sequential reactions

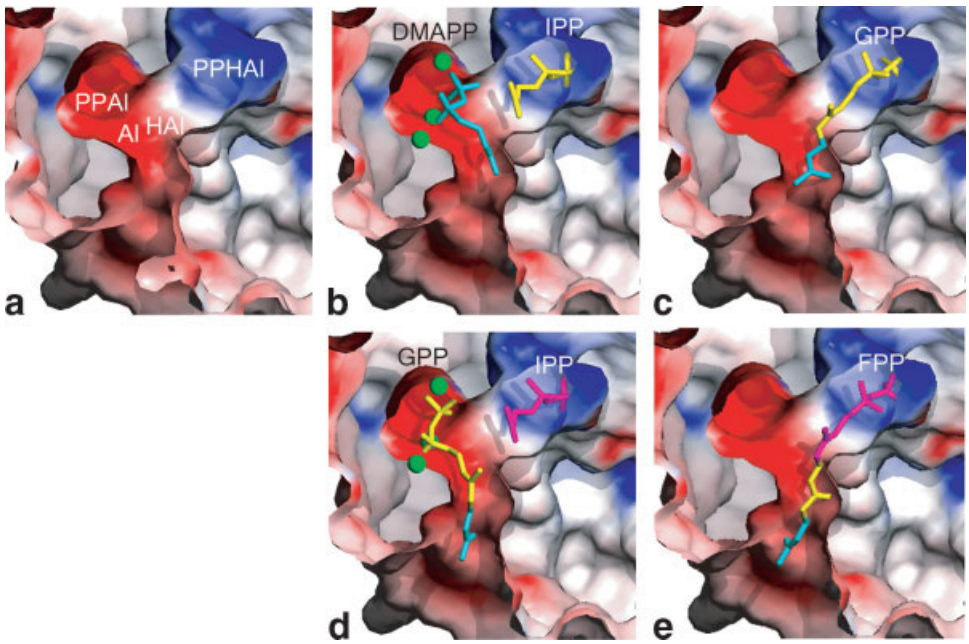

Fig. 5. Model of the binding of substrates and products to *Tc*FPPS. A cut of the binding site in the closed conformation is shown as an electrostatic surface calculated with GRASP. (**a**) The four subsites are labeled as Al (allyl), AlPP (allylic pyrophosphate), HAl (homoallyl), and HAlPP (homoallylic pyrophosphate) (see text). (**b**) Model of IPP (yellow) and DMAPP (blue) bound to *Tc*FPPS. The three magnesium ions are shown as green spheres. (**c**) Model of the geranyl diphosphate (GPP, yellow and blue) bound to the product binding site. The diphosphate and the magnesium ions have been released from the enzyme. (**d**) Model of FPPS-bound IPP and with GPP bound in the allylic site. The magnesium ions are shown in green. (**e**) Model of FPP bound to the product site.

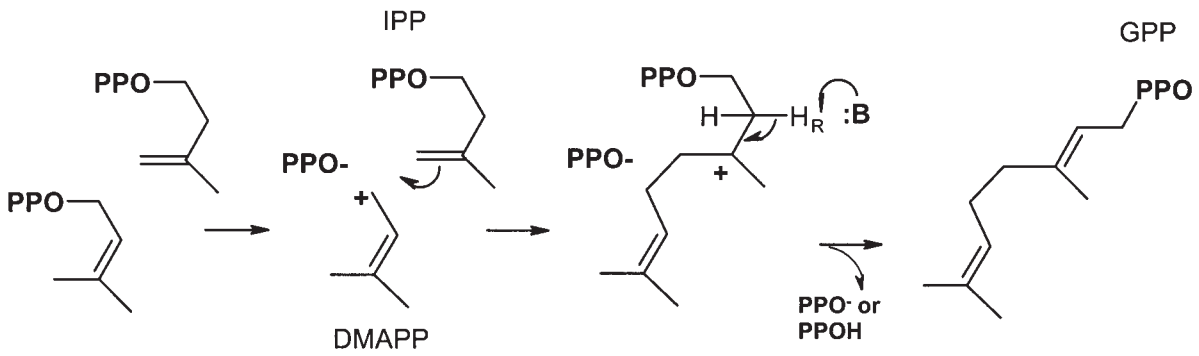

Scheme. 1.

carried out by FPPS may take place without release of the product of the first reaction. The condensation of DMAPP and IPP starts with the reactants occupying subsites PPAl, Al, PPHAl, and HAl, as described in the previous section [Fig. 5(b)]. After formation of the C—C bond, the release of the pyrophosphate of DMAPP, and the subsequent rearrangements, the resulting GPP can occupy subsites Al, HAl, and PPHAl, with only small changes in the positions of the atoms with respect to those of the precatalytic complex [Fig. 5(c)]. [The closed conformation of the enzyme does not have a clear path for the release of the pyrophosphate. More likely, the pyrophosphate is released from the open conformation of the enzyme, Fig. 2(c, d).] It is possible that the resulting GPP may be released from the enzyme and later be rebounded to participate in the second condensation. The available structures, however, suggest another possibility for the elongation of the GPP: in the presence of Mg^{2+} ions, the pyrophosphate of GPP may swing from the PPHAl subsite to the PPAl subsite, pivoting around the middle of the carbon chain [Fig. 5(d)]. For this to happen, two residues that separate subsites PPAl and PPHAl (Arg 107 and Lys 264) have to move out the way. This movement probably occurs when these two residues move to follow the pyrophosphate of the DMAPP as it leaves the enzyme. After the GPP pyrophosphate moves to subsite PPAl, the last five carbons of the GPP move to the Al subsite and allow a new IPP to bind to the PPHAl and HAl subsites to complete the second reaction [Fig. 5(e, f)].

Implications for Drug Design

The available inhibitors of FPPS bind to the enzyme occupying mainly subsites Al and PPAl. As discussed in the previous section, GPP may bind to the enzyme spanning subsites Al, HAl, and PPHAl. One can envision a bisphosphonate inhibitor that spans these subsites. Or, even better—because known inhibitors seem to prefer the PPAl site for bisphosphonate binding—would be an inhibitor that spans subsites PPAl, Al, and HAl. The fact that the group binding to subsite Al has to be planar while that binding to subsite HAl may have a nonplanar dihedral should provide a guide for this design.

METHODS

Cloning

The gene of the FPPS from *T. cruzi* was cloned into the *pET-28a+* vector as a fusion protein with a 6× histidine tag. The construct was transformed into *E. coli* BL21 (DE3) lysogenic competent cells as described before.[9]

Protein Expression

Recombinant *T. cruzi* pET28-FPPS was grown in LB media in the presence of kanamycin. Cultures were incubated at 37°C until they reached an OD_{600} of 0.9, at which time IPTG was added to a final concentration of 1 mM. After 3 h, cells were harvested by centrifugation at 5000 rpm for 12 min. The pellet was washed with 50 mM Tris pH 7.5, 0.5% KCl, 0.5% NaCl w/v. Pellets resuspended in 50 mM NaH_2PO_4, 50 mM NaCl, 10 mM imidazole, and 1 mM TCEP (Tris-2-carboxyethyl-phosphine hydrochloride), were lysed using a microfluidizer and centrifuged at 12000 rpm for 35 min. The supernatant was filtered through a 0.22-micron Millipore Stericup to remove debris.

The selenomethionyl substituted protein was expressed in the *E. coli* methionine auxotrophic strain B834 (DE3) (Novagen). Transformed cells were grown in minimal media supplemented with selenomethionine (Sigma).

Protein Purification

The protein was purified using a HisTrap Ni^{2+} chelate affinity column. For this, 250 mL of lysate were loaded onto the column and eluted with two successive linear imidazole gradients (10–50 mM; 50–250 mM). Pooled fractions were concentrated and dialyzed against 2 L of 20 mM Tris pH 7.9, 50 mM NaCl, 2 mM TCEP. Concentrated TcFPPS was digested with thrombin overnight at room temperature. The solution was diluted using a low salt buffer (20 mM Tris pH 7.9, 10 mM NaCl, 1 mM TCEP) and injected onto a preequilibrated Mono Q column. Fractions were eluted with a high salt buffer (20 mM Tris pH 7.9, 250 mM NaCl, 1 mM TCEP), pooled, concentrated to 50 mg/mL, and dialyzed against 20 mM Tris pH 7.9, 50 mM NaCl, 2 mM TCEP. Samples run on a 4–20% SDS-PAGE gel (or 8–16%) showed a single band of the expected molecular weight, when stained with Coomassie Blue.

Crystallization

A full search of crystallization conditions was carried out using an incomplete factorial set of conditions.[21] Using recently prepared protein and the presence of the reducing agent TCEP were crucial for diffraction quality crystals. Crystals used in data collection were produced by free-boundary diffusion in a narrow liquid bridge connecting the protein and the precipitant drops (0.2–0.4 M $(NH_4)_2SO_4$, 7.5–20% PEG 4000, 100 mM Na-acetate pH 4.6). Crystals appear within 1 h but their diffraction quality started to deteriorate after 2–3 days. Crystals were frozen within 2–3 days after addition of 1:4 glycerol: reservoir solution (by volume).

Preparation of FPPS, Risedronate, DMAPP, and Mg^{2+} Crystals

This complex of *Tc*FPPS was prepared by soaking a thawed native crystal for 45 min in mother liquor containing of 4 mM risedronate, 4 mM DMAPP, and 2 mM $MgCl_2$.

Preparation of FPPS, Alendronate, IPP, and Mg^{2+} Crystals

Selenomethionine substituted protein at 25 mg/mL was mixed with 4 mM alendronate, 4 mM IPP, 2 mM $MgCl_2$ for 30 min at room temperature before setting up the drops. Two microliters of these solutions were connected with a narrow liquid bridge to 2 μL of precipitant solution (100 mM Sodium Acetate pH 4.6, 200 mM Ammonium Sulfate, 2–10% PEG 4000). Fifty microliters of precipitant solution were placed in the reservoir to prevent drying of the drops. Crystals were flash frozen in 1:4 glycerol:reservoir solution.

Data Collection

Native *Tc*FPPS diffraction data were collected at beamline X4a of the National Synchrotron Light Source (NSLS) of the Brookhaven National Laboratory. Diffraction data were collected from a single frozen crystal (100 K) using a CCD-based detector. Data were processed and scaled using the HKL 2000 suite (Table I). In addition, a MAD data set was collected with a selenomethionine-containing crystal at three wavelengths around the selenium edge.[22] These data were collected with a Quantum 315 ADSC CCD-based detector at beamline X25 of the NSLS. X-ray diffraction statistics are summarized in Table I.

Structure Determination

Determination of the structure of the *Tc*FPPS was first attempted by molecular replacement using the coordinates of the structure of the FPPS from chicken (~30% sequence identity) as the search model. Although a solution was found, further model building and refinement failed to give a well-behaved, well-refined structure of the *Tc*FPPS. MAD phasing with selenomethionine-containing *Tc*FPPS looked particularly promising, because the enzyme contains 15 methionines (in 362 residues), six of them highly conserved. The positions of the anomalous scatterers, phasing, and density modification were successfully carried out using the programs SOLVE and RESOLVE.[23]

Model Building and Refinement

The model was built with the program O,[24] using as a guide the coordinates of the partial model built by RESOLVE. Refinement was carried out with CNS[25] and REFMAC;[26,27] progress of the refinement was monitored by following the conventional *R*-value and an *R*-free calculated with a crossvalidation set containing 5% of the reflections. The overall quality of the final model was assessed using the programs PROCHECK[28] and WHATIF.[27]

Structure of the FPPS Complexes

X-ray diffraction data were collected at beamline X25 of the NSLS and the structures determined either by direct refinement or by molecular replacement using the coordinates of the apoenzyme. Refinement of the structures was carried out with the programs CNS[25] and REFMAC.[27] The inhibitors, substrates, and metals were built in $2F_o - F_c$ maps, calculated with phases based on the protein atoms only.

Modeling

The structures of the complexes of avian[13,29] (1UBX, 1UBW), *E. coli*[14] (1RQI, 1RQJ), and *T. cruzi* (this work) enzymes were structurally aligned using the program SSM-EBI.[30] The alignment was improved with the least square program of the Uppsala Software Factory (USF) using only the two conserved regions containing the DDXXD motives. Models were built using the program Quanta (Accelerys, Inc.). The final models were subjected to a local energy minimization to eliminate unfavorable interactions between the substrate and the FPPS. Models of the *Tc*FPPS–Mg^{+2}–IPP–DMAPP and *Tc*FPPS–Mg^{+2}–IPP–GPP were built based on the structure of the *Tc*FPPS–Mg^{+2}–IPP–alendronate crystal and the position of the dimethylallyl-S-thiolodiphosphate in the *E. coli* structure (1RQI). The positions of GPP and FPP as products, in the homoallylic site, were modeled based on the coordinates of bound IPP.

Deposition of Atomic Coordinates

All coordinates have been deposited in the Protein Data Bank (accession code 1YHK, 1YHL, and 1YHM).

ACKNOWLEDGMENTS

The authors are grateful to Drs. D. Leahy and S. Bouyain for native data collection, and Drs. J. Sacchettini, A.S. Mildvan, and Mario A. Bianchet for helpful discussions. Data were collected at beamlines X4a and X25 of the National Synchrotron Light Source at the Brookhaven National Laboratory.

REFERENCES

1. WHO. TDR tropical disease research. www.who.int/tdr/. WHO International; 2004.
2. Barrett MP, Burchmore RJ, Stich A, Lazzari JO, Frasch AC,

Cazzulo JJ, Krishna S. The trypanosomiases. Lancet 2003;362: 1469–1480.
3. Brener Z. Present status of chemotherapy and chemoprophylaxis of human trypanosomiasis in the Western Hemisphere. Pharmacol Ther 1979;7:71–90.
4. Garzoni LR, Waghabi MC, Baptista MM, de Castro SL, Meirelles M de N, Britto CC, Docampo R, Oldfield E, Urbina JA. Antiparasitic activity of risedronate in a murine model of acute Chagas' disease. Int J Antimicrob Agents 2004;23:286–290.
5. Garzoni LR, Caldera A, Meirelles Mde N, de Castro SL, Docampo R, Meints GA, Oldfield E, Urbina JA. Selective in vitro effects of the farnesyl pyrophosphate synthase inhibitor risedronate on *Trypanosoma cruzi*. Int J Antimicrob Agents 2004;23:273–285.
6. Thompson K, Dunford JE, Ebetino FH, Rogers MJ. Identification of a bisphosphonate that inhibits isopentenyl diphosphate isomerase and farnesyl diphosphate synthase. Biochem Biophys Res Commun 2002;290:869–873.
7. Rogers MJ. New insights into the molecular mechanisms of action of bisphosphonates. Curr Pharm Des 2003;9:2643–2658.
8. Keller RK, Fliesler SJ. Mechanism of aminobisphosphonate action: characterization of alendronate inhibition of the isoprenoid pathway. Biochem Biophys Res Commun 1999;266:560–563.
9. Montalvetti A, Bailey BN, Martin MB, Severin GW, Oldfield E, Docampo R. Bisphosphonates are potent inhibitors of *Trypanosoma cruzi* farnesyl pyrophosphate synthase. J Biol Chem 2001; 276:33930–33937.
10. Martin MB, Grimley JS, Lewis JC, Heath HT 3rd, Bailey BN, Kendrick H, Yardley V, Caldera A, Lira R, Urbina JA, Moreno SN, Docampo R, Croft SL, Oldfield E. Bisphosphonates inhibit the growth of *Trypanosoma brucei*, *Trypanosoma cruzi*, *Leishmania donovani*, *Toxoplasma gondii*, and *Plasmodium falciparum*: a potential route to chemotherapy. J Med Chem 2001;44:909–916.
11. Urbina JA, Moreno B, Vierkotter S, Oldfield E, Payares G, Sanoja C, Bailey BN, Yan W, Scott DA, Moreno SN, Docampo R. *Trypanosoma cruzi* contains major pyrophosphate stores, and its growth in vitro and in vivo is blocked by pyrophosphate analogs. J Biol Chem 1999;274:33609–33615.
12. Szajnman SH, Montalvetti A, Wang Y, Docampo R, Rodriguez JB. Bisphosphonates derived from fatty acids are potent inhibitors of *Trypanosoma cruzi* farnesyl pyrophosphate synthase. Bioorg Med Chem Lett 2003;13:3231–3235.
13. Tarshis LC, Yan M, Poulter CD, Sacchettini JC. Crystal structure of recombinant farnesyl diphosphate synthase at 2.6-A resolution. Biochemistry 1994;33:10871–10877.
14. Hosfield DJ, Zhang Y, Dougan DR, Broun A, Tari LW, Swanson RV, Finn J. Structural basis for bisphosphonate-mediated inhibition of isoprenoid biosynthesis. J Biol Chem 2004;279:8526–8529.
15. Mao J, Gao YG, Odeh S, Robinson H, Montalvetti A, Docampo R, Oldfield E. Crystallization and preliminary X-ray diffraction study of the farnesyl diphosphate synthase from *Trypanosoma brucei*. Acta Crystallogr D Biol Crystallogr 2004;60(Pt 10):1863–1866.
16. Ogura K, Koyama T. Enzymatic aspects of isoprenoid chain elongation. Chem Rev 1998;98:1263–1276.
17. King H, Rilling H. Avian liver prenyltransferase. The role of metal in substrate binding and the orientation of substrates during catalysis. Biochemistry 1977;16:3815–3819.
18. Reed B, Rilling H. Substrate binding of avian liver prenyltransferase. Biochemistry 1976;15:3739–3745.
19. Cornforth JW, Cornforth RH, Popjak G, Yenguyan L. Studies in the biosynthesis of cholesterol. Steric course of carboxylation of 5-pyrophosphomevalonate and of the carbon to carbon bond formation in the biosynthesis of farnesyl pyrophosphate. J Biol Chem 1966;241:3970–3987.
20. Poulter CD, Satterwhite DM. Mechanism of the prenyl-transfer reaction. Studies with (E)- and (Z)-3-trifluoromethyl-2-buten-1-yl pyrophosphate. Biochemistry 1977;16:5470–5478.
21. Jancarik J, Kim, SH. Sparse matrix sampling:a screening method for crystallization of proteins. J Applied Crystallogr 1991;24:409.
22. Otwinowski Z, Minor W. Processing of X-ray diffraction data collected in oscillation mode. In: Carter CW Jr., Sweet RM, editors. Methods in Enzymology, Volume 276: Macromolecular Crystallography, part A. San Diego, CA: Academic Press; 1997. p. 307–326.
23. Terwilliger TC. SOLVE and RESOLVE: automated structure solution and density modification. Methods Enzymol 2003;374:22–37.
24. Jones TA, Zou JY, Cowan SW, Kjelgaard M. Improved methods for building protein models to electron density maps and the location of errors in these models. Acta Crystallogr A 1991;42:110–119.
25. Brunger AT, Adams PD, Clore GM, DeLano WL, Gros P, Grosse-Kunstleve RW, Jiang J, Kuszewski J, Nilges M, Pannu NS, Read R, Rice LM, Simonson T, Warren GL. Crystallography & NMR system: a new software suite for macromolecular structure determination. Acta Crystallogr D 1998;54:905–921.
26. Murshudov GN, Vagin AA, Dodson EJ. Refinement of macromolecular structures by the maximum-likelihood method. Acta Crystallogr D Biol Crystallogr 1997;53(Pt 3):240–255.
27. CCP4. The CCP4 suite: programs for protein crystallography. Acta Crystallogr D 1994;50:760–763.
28. Laskowski R, MacArthur M, Moss D, Thornton J. PROCHECK: a program to check the stereochemical quality of protein structures. J Appl Crystallogr 1993;26:283–291.
29. Tarshis LC, Proteau PJ, Kellogg BA, Sacchettini JC, Poulter CD. Regulation of product chain length by isoprenyl diphosphate synthases. Proc Natl Acad Sci USA 1996;93:15018–15023.
30. Krissinel E, Henrick K. Secondary-structure matching (SSM), a new tool for fast protein structure alignment in three dimensions. Acta Crystallogr D Biol Crystallogr 2004;60:2256–2258.